Lasers in Surgery and Medicine 9:148–154 (1989)

Light Distributions in Artery Tissue: Monte Carlo Simulations for Finite-Diameter Laser Beams

Marleen Keijzer, MSc, Steven L. Jacques, PhD, Scott A. Prahl, PhD, and Ashley J. Welch, PhD

Department of Dermatology, Wellman Laboratory, Harvard Medical School, Massachusetts General Hospital, Boston (M.K., S.L.J.), and Department of Electrical and Computer Engineering, Biomedical Engineering Program, The University of Texas at Austin, Austin (S.A.P., A.J.W.)

Finite-width light distributions in arterial tissue during Argon laser irradiation (476 nm) are simulated using the Monte Carlo method. Edge effects caused by radial diffusion of the light extend ±1.5 mm inward from the perimeter of a uniform incident beam. For beam diameters exceeding 3 mm the light distribution along the central axis can be described by the one-dimensional solution for an infinitely wide beam. The overlapping edge effects for beam diameters smaller than 3 mm reduce the penetration of the irradiance in the tissue. The beam profile influences the light distribution significantly. The fluence rates near the surface for a Gaussian beam are two times higher on the central axis and decrease faster radially than for a flat profile. The diverging light from a fiber penetrates tissue in a manner similar to collimated light.

Key words: absorption, aorta, dosimetry, fiber optics, lasers, photometry, random walk, scattering, radiation

INTRODUCTION

When using laser light in medical treatments, the rates of photochemical and thermal reactions depend on the light dose in the tissue. The distribution of the light within the tissue must be estimated from the irradiance delivered at the surface. To predict the internal light dose in turbid tissue an understanding of radiative transport in scattering media is required.

The most commonly used description of light propagation in highly scattering media is the equation of transfer [1]. This equation has only been solved for a one-dimensional geometry. Two- and three-dimensional solutions require a serious restriction of the angular distribution of the scattered light [2]. Examples of approximations that provide three-dimensional light distributions are the diffusion approximation [3,4] and the seven-flux model [5].

When treating the highly forward-directed light scattering characteristic of tissues [6,7], the validity of the diffusion approximation is suspect [8]. The transition from a collimated laser beam, incident at the surface, to a diffuse flux, deeper in the tissue, occurs in the first several hundred microns of tissue. This is the region that is most important for many laser/tissue interactions yet where the light distributions are the least accurately described by diffusion theory [9].

An alternative to solving the equation of

Accepted for publication December 15, 1988.

Scott A. Prahl is now at the Experimental Laser Unit, Academic Medical Center, 1105 AZ Amsterdam, the Netherlands.

Ashley J. Welch is the Marion E. Forsman Centennial Professor of Electrical and Computer Engineering and Biomedical Engineering.

Steven L. Jacques and Marleen Keijzer are now at the Laser Biology Research Laboratory, Box 17, MD Anderson Cancer Center, 1515 Holcombe Blvd., Houston, TX 77030. Address reprint requests there.

TABLE 1. Optical Parameters, Artery Media, 476 nm

μ_a = 6/cm	Absorption coefficient
μ_s = 414/cm	Scattering coefficient
μ_t = 420/cm	Total attenuation coefficient, $\mu_a + \mu_s$
g = 0.91	Mean cosine of the scattering angle
n = 1.37	Index of refraction

transfer is to simulate light propagation in a scattering medium with the Monte Carlo method [10–12]. Each photon out of a large sample is followed on its random walk until it is absorbed. The total light distribution is estimated from the resulting distribution of absorbed photons. With the Monte Carlo method, light transport can be calculated without approximating the tissue geometry or the angular distribution of light. The exact scattering properties can be simulated as well as the internal reflection at mismatched boundaries.

This paper presents a Monte Carlo simulation for the light distribution in human aorta irradiated with argon laser light (476 nm). The optical properties of normal human aorta at other wavelengths will be published elsewhere [13]. The effect of the beam diameter on the internal light distribution is discussed. The light distributions associated with a uniform beam, a Gaussian beam, and the slightly diverging light from an optical fiber are compared.

MATERIALS AND METHODS

Optical Parameters

The optical parameters used are those of the media of normal human aorta at 476 nm. The absorption coefficient, μ_a, the scattering coefficient, μ_s, and the mean cosine of the scattering angle, g, are listed in Table 1. The total attenuation coefficient, μ_t, is defined as the sum of μ_a and μ_s. The sample is 1.5 mm thick and is surrounded by air. The index of refraction of the sample is assumed to be 1.37 [7].

The optical parameters were obtained experimentally from one sample using the method of Jacques and Prahl [7], modified to include the delta-Eddington approximation of the scattering function [14]. The total attenuation coefficient, μ_t, was obtained by measuring on-axis transmission through thin sections of media (10–50 μm). Integrating sphere measurements of the total transmission and total reflection of the full-thickness sample yielded the remaining optical parameters.

Monte Carlo Method

In the Monte Carlo program, photons are multiply scattered as they propagate through the tissue until they are absorbed. Photons enter the tissue at a single point on the surface. The initial direction of the photons is sampled from the angular distribution of the incident beam. The advantage of having the photons entering through a single point is that the result constitutes a spatial impulse response, which can be convolved over any profile of the incident beam, thus eliminating the need for many lengthy Monte Carlo simulations.

The path of a photon in a scattering medium consists of steps of varying length between interaction sites and angles of deflection for scattering events. Every step length and scattering angle is sampled from its respective distribution (see below). To reduce the number of photons needed to estimate the actual light distribution, weighted photons are used. At each interaction site, μ_a/μ_t of the weight of the photon is deposited as absorbed energy, after which the photon is scattered into a new direction. When the weight of the photon has been reduced to 1/20,000th of its initial weight, the photon is "killed," and a new one is launched. (Instead of one photon losing weight to absorption along its path, the process can be thought of as a bundle of photons leaving a trail of absorbed photons behind.) When the photon hits the tissue/air boundary, part of the photon's weight is transmitted into the air according to Fresnel's laws for unpolarized light. The remaining weight is internally reflected and continues its random walk. The results presented are obtained by launching 20,000 photons.

Below, the random walk of the photons is described in more detail.

Sampling random variables. The principle of the Monte Carlo method is well described by Cashwell and Everett [15]. To determine the random walk of a photon, certain random variables, such as the path length between two scattering events or the scattering angle, must be assigned values at every interaction site. The values of the variable are chosen randomly from the distribution of the variable in the following way.

Define p(x) as the probability density function of a random variable x ($a \le x \le b$), where

$$\int_a^b p(x)\,dx = 1. \tag{1}$$

Then the sample, x_{rnd}, of the random variable x is

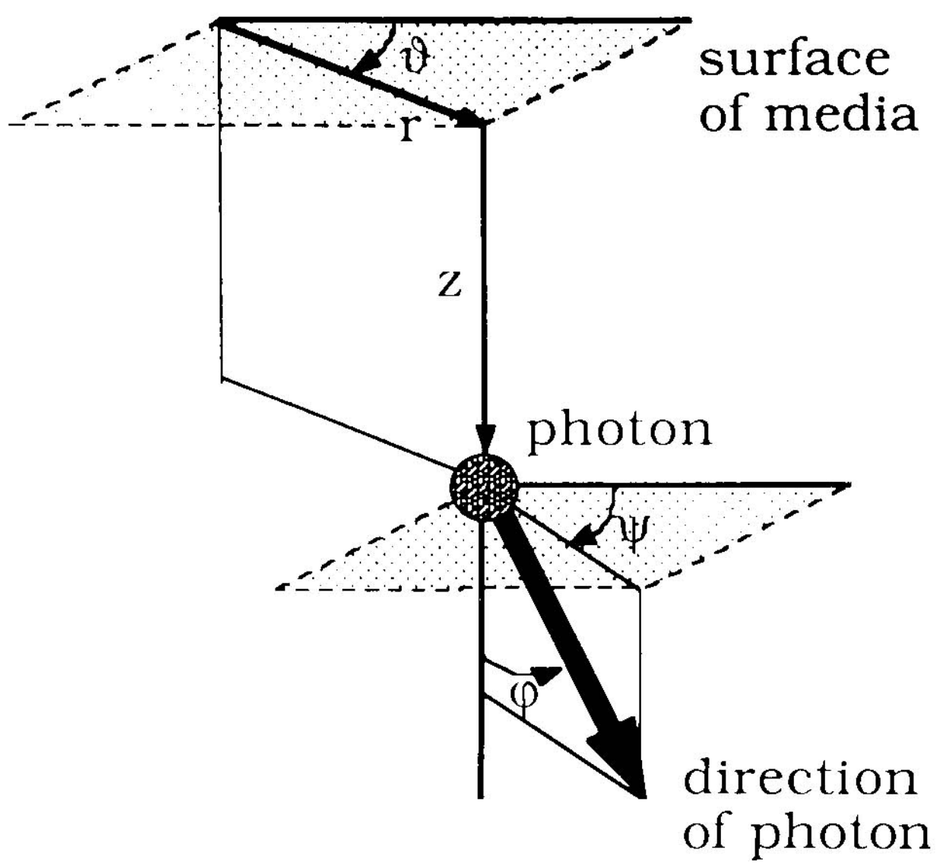

Fig. 1. Coordinates for random walk. $0 \le r$, $0 \le \vartheta \le 2\pi$, $0 \le z \le$ sample thickness, $0 \le \varphi \le \pi$, $0 \le \psi \le 2\pi$.

simulated by choosing a random number, RND, from a uniform distribution $0 \le RND \le 1$ and requiring

$$RND = \int_a^{x_{rnd}} p(x)\,dx. \tag{2}$$

Equation 2 is applied to a particular random variable, x, and rearranged, yielding x_{rnd} as a function of RND.

Coordinates. The coordinate system for the Monte Carlo simulation is shown in Figure 1. The position of the photons, **r**, is described in cylindrical coordinates, (r, ϑ, z) $(0 \le r,\ 0 \le \vartheta \le \pi,\ 0 \le z \le$ medium thickness), and the direction of the photons is described in spherical coordinates, (φ, ψ) $(0 \le \varphi \le \pi,\ 0 \le \psi \le 2\pi)$.

The photons migrate in three dimensions. However, we consider cylindrically symmetric geometries, and therefore the ϑ-dependence of the absorption can be ignored. The tissue is divided into a two-dimensional array in r and z, which specifies element volumes in which the absorbed weights of the propagating photons are recorded. These element volumes are logarithmically scaled: small near the source and large far from the source.

Random walk. Every generated path length between interaction sites, L $(L \ge 0)$, is calculated from a random number, RND, as described above. The probability density function, p(L), of the path length is

$$p(L) = \mu_t\, e^{-\mu_t L}, \tag{3}$$

where p(L) satisfies the normalization of equation 1. Substitution of equation 3 into equation 2 yields an expression for the path length sample, L_{rnd}:

$$L_{rnd} = -\ell n(1-RND)/\mu_t. \tag{4}$$

In this way L_{rnd} is selected by RND, which is generated by a random number generator.

The photon is displaced from the old position, (r, ϑ, z), over distance L (which is sampled by L_{rnd}), in direction (φ, ψ). The coordinates of the new position, (r', ϑ', z'), are

$$r' = (r^2 + 2rL\sin\varphi\cos(\psi-\vartheta) + (L\sin\varphi)^2)^{1/2}$$

$$\vartheta' = \begin{cases} \vartheta + \operatorname{asin}(L\sin\varphi\sin(\psi-\vartheta)/r', \\ \qquad \text{for } L\sin\varphi\cos(\pi-\psi+\vartheta) \le r \\ \vartheta + \pi + \operatorname{asin}(L\sin\varphi\sin(\psi-\vartheta)/r', \\ \qquad \text{for } L\sin\varphi\cos(\pi-\psi+\vartheta) > r \end{cases}$$

$$z' = z + L\cos\varphi. \tag{5}$$

At the new position, μ_a/μ_t of the weight of the photon is deposited in an element of the absorption array. The photon is then scattered with μ_s/μ_t of its former weight. We assume that the angle of deflection has a Henyey-Greenstein distribution [16], which, as Jacques et al [17] have demonstrated, well describes the light scattering in tissues:

$$p(\varphi_s) = \tfrac{1}{2}(1-g^2)/(1+g^2-2\,g\,\cos\varphi_s)^{3/2}$$

$$p(\psi_s) = \frac{1}{2\pi}, \tag{6}$$

where φ_s is the polar scattering angle $(0 \le \varphi_s \le \pi)$, and ψ_s is the azimuthal scattering angle $(0 \le \psi_s \le 2\pi)$. Probability density functions $p(\varphi_s)$ and $p(\psi_s)$ satisfy equation 1. Substitution of equations 6 into equation 2 yields relations to obtain the scattering angle samples $(\varphi_{s\,rnd}, \psi_{s\,rnd})$:

$$\varphi_{s\,rnd} = \operatorname{acos}\left(\frac{1}{2g}\left[1 + g^2 - \left(\frac{1-g^2}{1-g+2gRND}\right)^2\right]\right)$$

$$\psi_{s\,rnd} = 2\pi RND. \tag{7}$$

The deflection angle, (φ_s, ψ_s), is specified by the samples $\varphi_{s\ rnd}$ and $\psi_{s\ rnd}$. From the old direction, (φ, ψ), the photon is scattered over angle (φ_s, ψ_s) into direction (φ', ψ') according to the following relations [10]:

$$\varphi' = \operatorname{acos}(\cos\varphi_s \cos\varphi - \sin\varphi_s \sin\varphi \cos\psi_s)$$

$$\psi' = \begin{cases} \psi + \operatorname{atan}(\sin\varphi_s \sin\psi_s/\alpha), & \text{for } \alpha>0 \\ \psi + \operatorname{atan}(\sin\varphi_s \sin\psi_s/\alpha) \pm \pi, & \text{for } \alpha<0, \end{cases}$$

$$\text{where } \alpha = \cos\varphi_s \sin\phi + \sin\phi_s \cos\psi_s \cos\varphi. \quad (8)$$

If a photon strikes the surface, part of its weight is transmitted into the air according to Snell's law and Fresnel's equations for unpolarized light. The amount transmitted through the surface is added to the total reflection or total transmission. The remaining fraction of the photon is internally reflected and continues its random walk.

Spatial Impulse Response. The method yields the rate of energy deposition, $Q(\mathbf{r})$, in W/cc per unit of incident power (in W), that enters the sample through a single point on the surface. In other words, $Q(\mathbf{r})$ has unit 1/cc. The corresponding fluence rate distribution, the spatial impulse response, $G(\mathbf{r})$, is coupled to the rate of energy deposition, $Q(\mathbf{r})$, by the absorption coefficient, μ_a:

$$Q(\mathbf{r}) = \mu_a\, G(\mathbf{r}). \quad (9)$$

Therefore, the unit of the spatial impulse response in the tissue, $G(\mathbf{r})$, is $1/cm^2$, which allows the spatial impulse response to be convolved against an incident beam (see equation 10). This convolution yields $\Psi(\mathbf{r})$, the total fluence rate, in W/cm^2.

Two spatial impulse responses are used: one for collimated light incident perpendicularly to the surface and one for divergent light from a fiber with a numerical aperture of 0.26. The spatial impulse response, $G(\mathbf{r})$, for human aorta irradiated by a collimated 476-nm ray is given in Figure 2. The fluence rate directly under the beam is orders of magnitude higher than next to it. However, because of the large differences in volumes, the total amount of light scattered away from the central axis is far greater than the collimated light on axis.

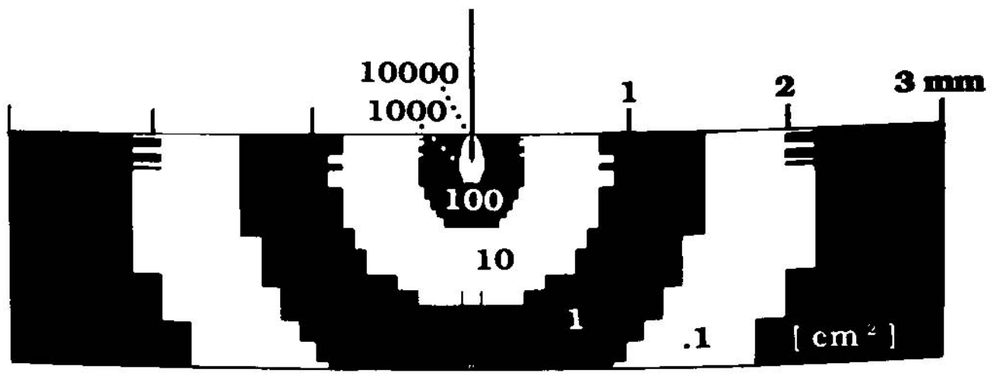

Fig. 2. Spatial impulse response, $G(\mathbf{r})$ in cm^{-2}, light distribution induced by a collimated ray through a point on the surface of tissue with parameters of Table 1. The light penetrates to form a narrow cylinder, then rapidly diffuses into a hemispherical pattern.

Finite beam convolution. The light distribution in the tissue, $\Psi(\mathbf{r})$, caused by a beam with an arbitrary irradiance profile, $E(r,\vartheta)$ in W/cm^2, is obtained by convolving the spatial impulse response, $G(\mathbf{r})$, with the source:

$$\Psi(r,\vartheta,z) = \int_0^{2\pi}\int_0^{\infty} E(r',\vartheta')\, G(\sqrt{r^2 + r'^2 - 2rr'\cos(\vartheta-\vartheta')},z)\, r'dr'd\vartheta'. \quad (10)$$

$E(r,\vartheta)$ is constant over the beam area for a flat beam profile. $E(r,\vartheta)$ is proportional to $\exp(-2(r/R_1)^2)$ for a Gaussian beam with a $1/e^2$ radius R_1.

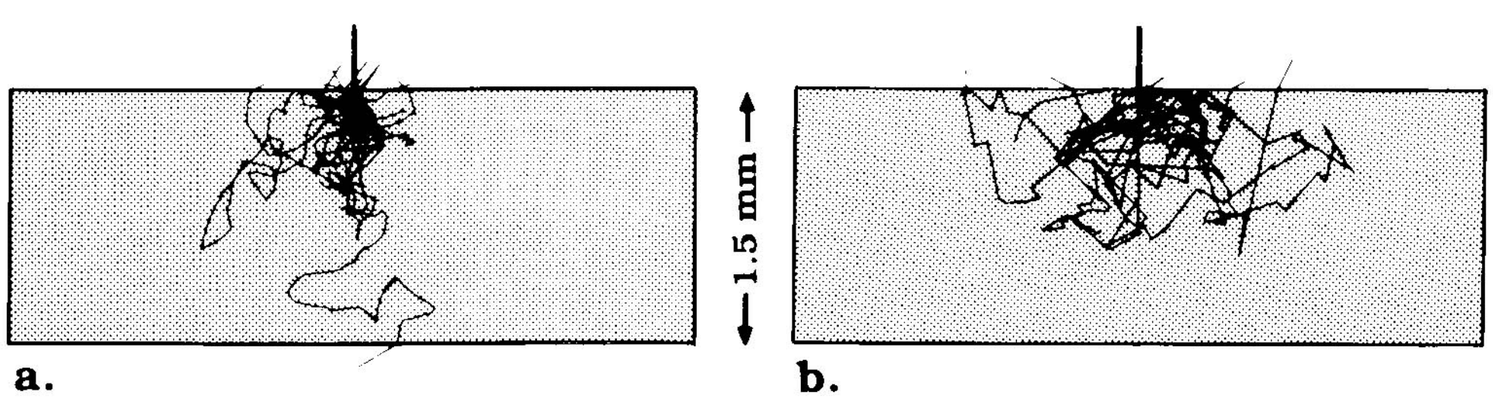

Fig. 3. Monte Carlo simulations of the propagation of photons in human aorta (30 photons shown). The internal light distribution is influenced by the scattering function. **a:** Henyey-Greenstein function, where $g = 0.91$, $\mu_s = 414/cm$. **b:** Isotropic scattering function where the similarity relation is conserved: $g = 0$, $\mu_s = 37.3/cm$.

RESULTS

Influence of the Scattering Function

The paths of 30 photons, generated by the Monte Carlo program, are projected on the $\varphi = 0$ plane in Figure 3. For reasons of clarity, the photons in Figure 3 are multiply scattered without losing weight until a single absorption event terminates propagation.

The consequences of changing the optical scattering parameters can directly be visualized with the Monte Carlo method. In Figure 3a, the photons are scattered according to the Henyey-Greenstein function (equations 6). In Figure 3b, the scattering function in tissue is approximated by an isotropic function ($g = 0$), according to the similarity relation. The similarity relation asserts that the penetration of light through a scattering media will remain constant, if the "reduced scattering coefficient," $\mu_s(1-g)$, is conserved [18, Chapter 14]. Therefore the scattering coefficient for the isotropic function in Figure 3b is chosen: $\mu_s' = \mu_s(1-g)$. The scattering angles in Figure 3b are much bigger, but more importantly, the whole pattern is wider. For a finite-diameter incident beam this pattern will result in a light distribution that is lower directly under the beam but spread out wider compared to the light distribution calculated with an anisotropic scattering function, as in Figure 3a.

Therefore, the details of the scattering function do influence the light distributions of beams of finite diameter. The Monte Carlo technique enables the Henyey-Greenstein function to be used, rather than an approximation.

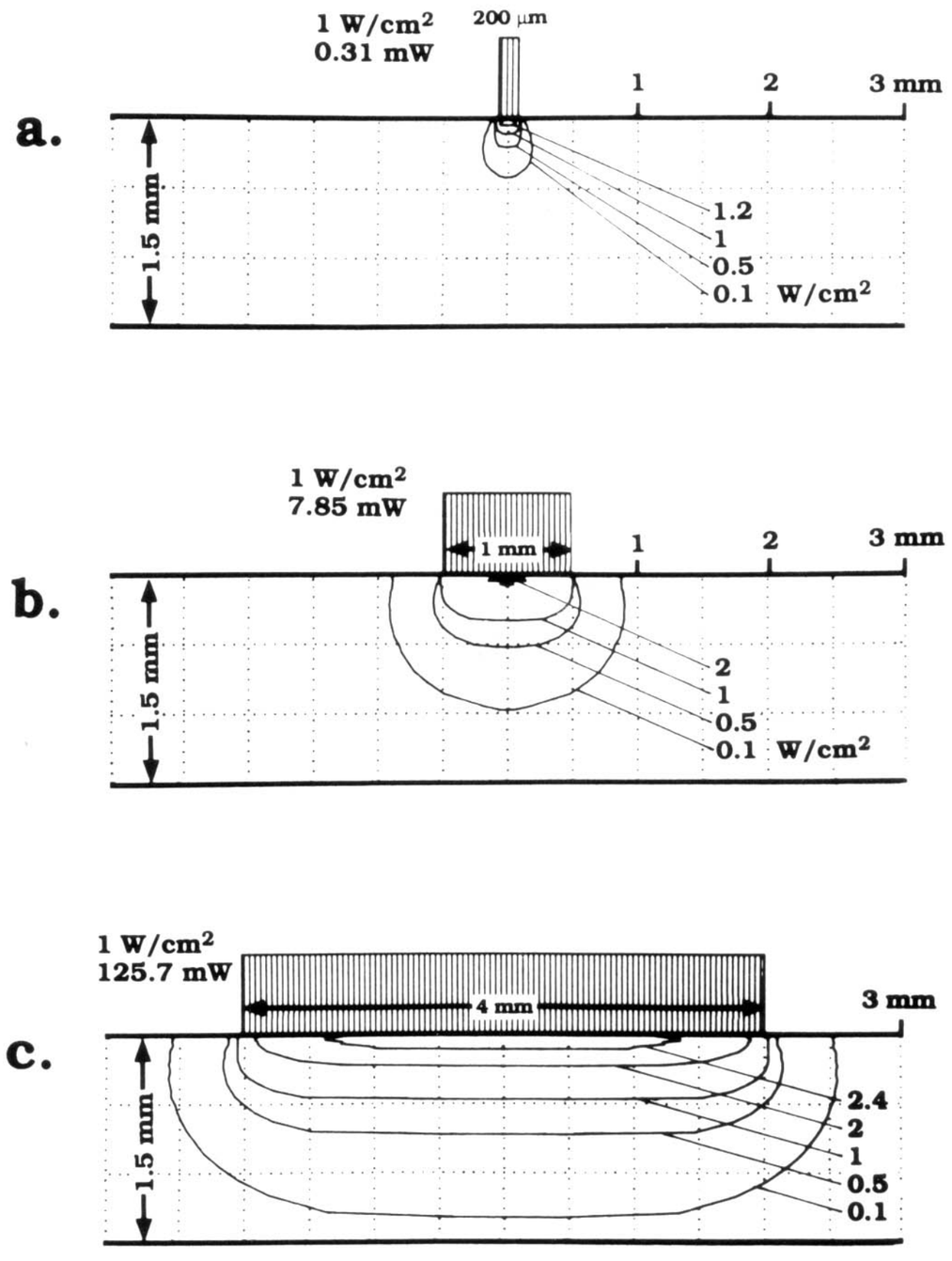

Fig. 4. Distributions of 476 nm light in human aorta for flat, collimated incident beams with different diameters (**a:** 200 μm; **b:** 1 mm; **c:** 4 mm). The power density of the incident beam is 1 W/cm^2. As shown in c, the edge effects extend ±1.5 mm from the perimeter of the beam inward, leaving a central cylinder of 1 mm diameter with a one-dimensional light distribution. The edge effects overlap in the center for beam diameters smaller than 3 mm, which decreases the penetration of light (a,b).

Effect of the Beam Diameter

Light distributions in arterial tissue in air for three diameters (200 μm, 1 mm, and 4 mm) of a uniform incident beam are shown in Figure 4. The incident irradiance in each figure is 1 W/cm^2. Back-scattered light augments the incident beam, yielding an internal fluence rate that exceeds the irradiance delivered at the surface. Directly under the incident beam, the light is still rather forward directed, as shown by the large radial gradient in fluence rate at the edge of the beam. Farther away from the source, the light is more diffuse.

Radial diffusion creates edge effects that extend ±1.5 mm from the perimeter of the incident beam inward. The light distribution associated with the 4 mm-wide beam (Fig. 4c) has a central cylinder of 1 mm diameter that is unaffected by the edge effects. Within this central cylinder, the fluence rates are the same as for an infinitely wide flat beam. When the incident beam is narrower than 3 mm, the edge effects overlap, decreasing the fluence rates in the center (Fig. 4a,b).

The maximum fluence rate is obtained on axis, below the surface. The depth of the maximum depends on the diameter of the incident beam. The maximum fluence rate for beam diameters over 3 mm is obtained at a depth of about 35 μm (Fig. 4c). As the beam diameter is decreased, the maximum moves toward the surface (Fig. 4a,b).

The magnitude of the maximum fluence rate also depends on the beam diameter. The maximum fluence rate for the 4 mm beam is almost 2.5

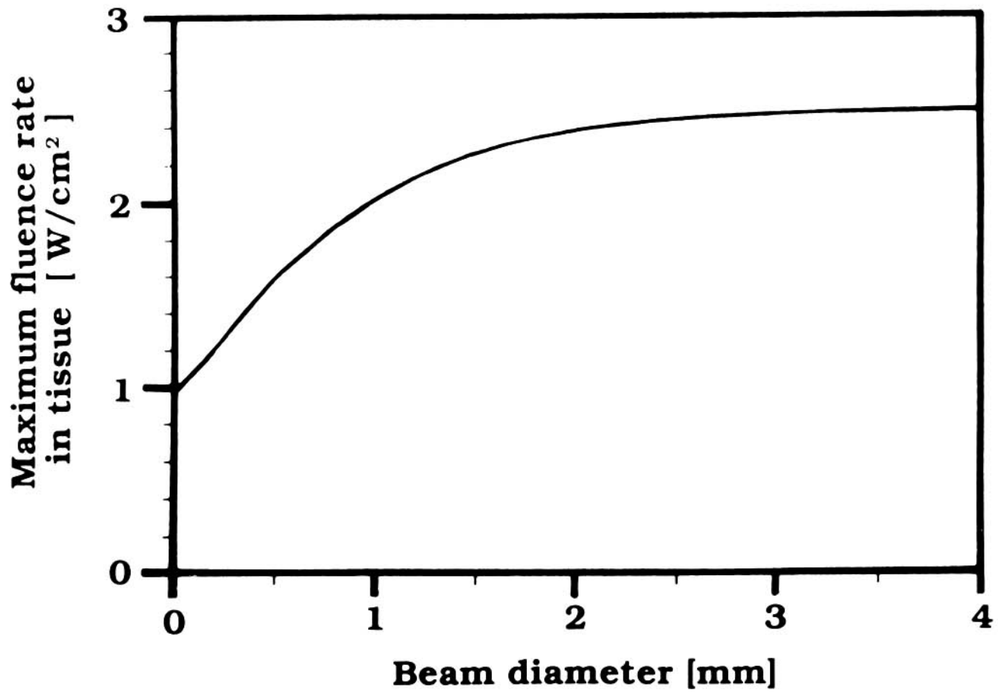

Fig. 5. Maximum fluence rate in the tissue as a function of the beam diameter. As the beam diameter decreases, the edge effects caused by scattering overlap, yielding lower fluence rates within the tissue. The position of the maximum is about 35 μm under the surface for beam diameters over 3 mm and moves toward the surface for decreasing diameters (476 nm, 1 W/cm^2 collimated beam with a flat profile, incident on human aorta).

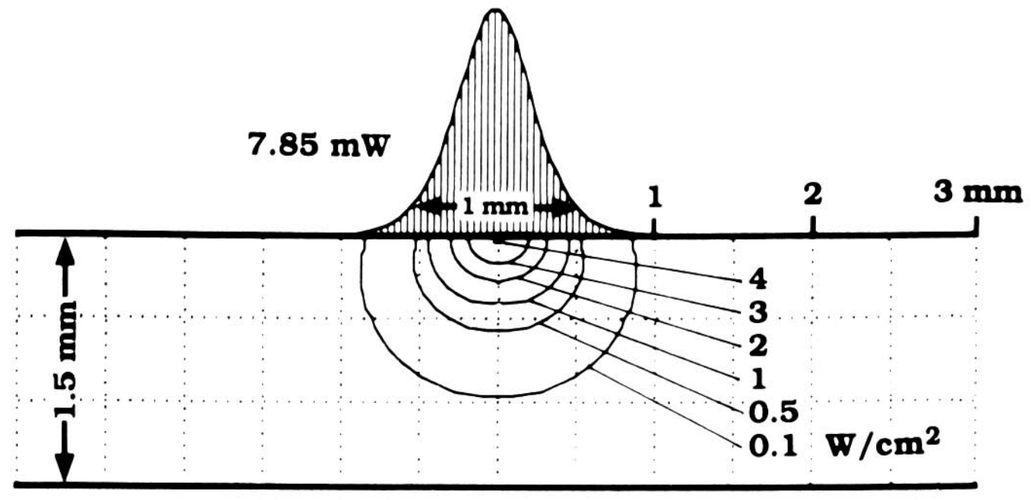

Fig. 6. Distribution of 476 nm light in human aorta for a collimated beam of 7.85 mW with a Gaussian profile ($1/e^2$ diameter of 1 mm). Compare this distribution to the distribution associated with a flat profile as in Figure 4b.

W/cm^2 (Fig. 4c). The maximum value for the 1 mm beam is 2 W/cm^2 (Fig. 4b) and for the 200 μm beam is 1.2 W/cm^2 (Fig. 4a). The magnitude of the maximum fluence rate depends on the beam diameter, as summarized in Figure 5. The maximum for the limit of a 0-diameter beam has the same magnitude as the incident irradiance, i.e., 1 W/cm^2.

The sample is surrounded by air. Internal reflection, caused by mismatched boundaries, increases the fluence rate near the surface almost to the subsurface maximum. However, for a sample of aorta submerged in water the fluence rate at the surface is about 20% lower than the subsurface maximum for broad beams.

Gaussian Beam

In Figure 4 the beam profile is flat. The light distribution induced by a beam with a Gaussian profile, with a $1/e^2$ diameter of 1 mm, is shown in Figure 6. The total beam power is 7.85 mW, which matches the power of the 1 mm flat beam in Figure 4b. The whole pattern for the Gaussian profile is rounder than the one for the flat profile. The maximum lays nearer to the surface and is less wide. The maximum fluence rate is 4 W/cm^2, twice as high as the one for a flat profile. The profile of the incident beam strongly influences the radial light distribution in the tissue.

Optical Fiber

Another means of delivery is an optical fiber. Instead of being perfectly collimated, the light coming out of a fiber has an angular distribution. The light distribution in the tissue calculated for a 200 μm diameter fiber with NA = 0.26, positioned just above the surface of the tissue, is shown in Figure 7. The angular distribution of the source is approximately Gaussian, with a standard deviation of 11 degrees [19].

Comparison of Figure 7 to Figure 4b demonstrates that the divergence of the fiber light has little effect on the light distribution in highly scattering tissue. There is additional radial broadening and reduced penetration, but the differences are not significant (the maximum difference is 0.08 W/cm^2). The distributions are even more similar for the case of a fiber in contact with the tissue, as index matching decreases the numerical aperture of the fiber.

DISCUSSION

Since the Monte Carlo program does not approximate the angular distribution of the light or the scattering function, light transport can be calculated with any required accuracy, even near sources and boundaries. (Elsewhere will be published a demonstration of the accuracy of the Monte Carlo method in predicting measured light distributions [13, 20].) Furthermore, no restrictions are placed on the geometry of tissue and incident beam. Inhomogeneities such as blood vessels imbedded in tissue and the layered structure of skin can be included in a straightforward manner. One can simulate any laser beam profile

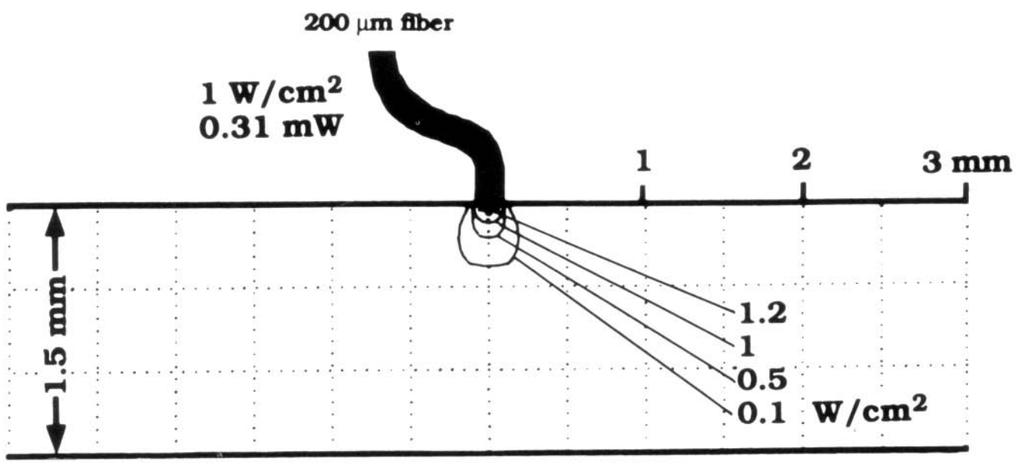

Fig. 7. Distribution of 476 nm light in human aorta for an optical fiber with NA = 0.26 and a diameter of 200 μm. The source is 1 W/cm^2, 0.31 mW. Compare this distribution for a divergent beam to the distribution induced by a collimated beam as in Figure 4a.

and the dispersion of the light from any fiber tip, either positioned inside the tissue or outside.

Monte Carlo calculations take too long to be used for immediate calculations during an experiment or treatment. However, the results of the calculations for a range of optical parameters can be stored for quick recall during procedures.

By comparing light distributions calculated with approximations to the transport equation (e.g., the diffusion equation) with the results of the Monte Carlo calculations, the former methods can be tested, and their systematic errors can be specified. Thus, light propagation models can be tested for their ability to obtain the tissue optical properties [e.g. 7] and to predict light distributions.

The results presented demonstrate that the internal light dose strongly depends on the diameter and the profile of the incident beam. Broad beams, for example surface irradiation during photodynamic therapy with conventional light sources or expanded laser beams, are well described by the one-dimensional solution (the central cylinder in Fig. 4c). However, narrow laser beam and optical fiber delivery require consideration of the beam diameter dependence of the internal light dose.

ACKNOWLEDGMENTS

This work was funded in part by the National Institutes of Health, grant AM25395-08, the Office of Naval Research under contract #N00014-86-K-00116 and #N00014-86-K-0875 and the Whitaker Health Sciences Fund.

REFERENCES

1. Chandrasekhar S: "Radiative Transfer." London: Oxford Univ. Press, 1950.
2. Case KM, Zweifel PF: "Linear Transport Theory." Reading, MA: Addison-Wesley, 1969.
3. Ishimaru A: "Wave Propagation and Scattering in Random Media," Volume 1. New York: Academic Press, 1978.
4. Keijzer M, Star WM, Storchi PRM: Optical diffusion in layered media. Appl Optics 1988; 27:1820–1824.
5. Yoon G, Welch AJ, Motamedi M, van Gemert MCJ: Development and application of three-dimensional light distribution model for laser irradiated tissue. IEEE J Quantum Electron 1987; QE-23:1721–1733.
6. Flock ST, Wilson BC, Patterson MS: Total attenuation coefficients and scattering phase functions of tissues and phantom materials at 633 nm. Med Phys 1987; 14:835–841.
7. Jacques SL, Prahl SA: Modeling optical and thermal distributions in tissue during laser irradiation. Lasers Surg Med 1987; 6:494–503.
8. Furutsu K: Diffusion equation derived from space time transport equation. J Opt Soc Am [A] 1980; 70:360–366.
9. Ishimaru A, Kuga Y, Cheung R L-T, Shimizu K: Scattering and diffusion of a beam wave in randomly distributed scatterers. J Opt Soc Am [A] 1983; 73:131–136.
10. de Belder M, de Kerf J, Jespers J, Verbrugge R: Light diffusion in photographic layers: Its influence on sensitivity and modulation transfer. J Opt Soc Am [A] 1965; 55:1261–1268.
11. Witt AN: Multiple scattering in reflection nebulae I-IV. Astroph J [Suppl] 1977; 55:1–36.
12. Wilson BC, Adam G: A Monte Carlo model for the absorption and flux distributions of light in tissue. Med Phys 1983; 10:824–830.
13. Keijzer M, Richards-Kortum RR, Jacques SL, Feld M: Fluorescence spectroscopy of turbid media: Autofluorescence of human aorta (in preparation).
14. Joseph JH, Wiscombe WJ: The Delta-Eddington approximation for radiative flux transfer. J Atm Sci 1976; 33: 2452–2459.
15. Cashwell ED, Everett CJ: "A Practical Manual on the Monte Carlo Method for Random Walk Problems." New York: Pergamon, 1959.
16. Henyey LG, Greenstein JL: Diffuse radiation in the galaxy. Astroph J 1941; 93:70.
17. Jacques SL, Alter CA, Prahl SA: Angular dependence of HeNe laser light scattering by human dermis. Lasers Life Sci 1987; 1:309–333.
18. van de Hulst HC: "Multiple Light Scattering," Volume II. New York: Academic Press, 1980.
19. Schroeder G: "Technische Optik." Wuerzburg: Vogel, 1984.
20. Jacques SL, Keijzer M, Marijnissen H, Star WM: Light distributions in phantom tissues: Theory meets experiment (in preparation).